ATLAS
MATERIAL TESTING SOLUTIONS

1915
Solar
Determinator®

1927
Original
Weather-Ometer®

1954
Xenotest® 150

1977
Ci65 Weather-Ometer®

1995
Ci4000
Weather-Ometer®

TODAY
The Ci4400
Weather-Ometer®

Our Latest Milestone. The Atlas Ci4400.

For over 100 years, we've revolutionized the science of weather durability testing. The new Atlas Ci4400 Weather-Ometer® is our most advanced instrument yet, delivering unparalleled performance and value. With its simplified operation, unmatched uniformity, increased capacity and sleek design, the best-in-class just got even better. Learn more at **atlas-mts.com**.

AMETEK®
MEASUREMENT, COMMUNICATIONS
& TESTING

JOURNAL OF Applied Polymer SCIENCE

Preparation and characterization of shape memory composite foams based on solid foaming method

Y. Yao,[1] T. Zhou,[1] Y. Xu,[1] Y. Liu,[2] J. Leng[1]

[1]Science and Technology on Advanced Composites in Special Environments Laboratory, Harbin Institute of Technology, Harbin 150080, China

[2]Department of Astronautical Science and Mechanics, Harbin Institute of Technology (HIT), Harbin 150001, China

Correspondence to: J. Leng (E-mail: lengjs@hit.edu.cn)

ABSTRACT: As we know, shape-memory foams with porous feature are better suited for a certain application compared with their solid counterparts, especially in tissue engineering, drug delivery, filtration, etc. In this study, a type of biocompatible composite foam with shape-memory property has been developed on the basis of biocompatible materials cross-linked poly(ε-caprolactone) (PCL) and silk fibrin (SF). Solid-state foaming method was used to fabricate the composite shape-memory foam. Hierarchical cellular foam with micropore on the cellular wall was observed. To optimize pore morphology, the relationship between cross-linking agent content/reinforcement filler content and PCL matrix was investigated. Excellent shape-recovery property (>97.6%) and shape-fixing property (>98%) have been achieved for PCL foam. For composite foams, SF addition is not too much effective on their shape-memory property by varying SF content. © 2018 Wiley Periodicals, Inc. J. Appl. Polym. Sci. **2018**, *135*, 46767.

KEYWORDS: composite foam; shape memory effect; shape memory foam

Received 25 December 2017; accepted 27 May 2018

DOI: 10.1002/app.46767

INTRODUCTION

The porous structure feature and shape-memory characteristic to make the shape-memory foams have properties such as lightweight, high-compressive ratio, deformation, storage strain energy, and multi-actuation method. Because of such unique features, it attracted intensive academic and industrial interests. Its structure and mechanical property with tunable behavior could be applied in actuator, sensor, and smart structures in the fields of aerospace engineering, biomedical engineering, and smart textile.[1–10] For example, Santo and co-workers produced shape-memory polymer (SMP) foams via solid state foaming method, which have been carried out experiments in two aeronautical missions.[11,12] Zhang et al. prepared inorganic–organic SMP foams containing inorganic polydimethylsiloxane (PDMS) segments and organic poly(ε-caprolactone) (PCL) segments.[13] The PDMS segments acted as soft segments whereas PCL segments served as switching segments. By varying the length of PDMS segments, SMP foams showed tunable properties, including porosity, pore size, degradation rate, and compressive modulus. Leng et al. adopted the microwave heating, to rapidly foam and actuate biocompatible shape-memory cross-linked PCL foams, displaying the excellent shape recovery of approximate 100% in 98 s.[14]

Among various applications, the biomedical applications of SMP porous structure attracted increasing interests because of its unique features of active volumetric and structural transformations, which allow them meet special needs for minimally invasive surgeries as embolic vascular devices, drug delivery platforms, and scaffolds for tissue engineering, etc.[15–18] Take an example, Maitland et al. reported that polyurethane-based shape-memory closed-cell foams could be used to fill intracranial aneurysms, preventing blood from flowing into the aneurysm, reducing the formation of thrombus to avoid the rupture of aneurysms.[18] In addition, Zhang et al. developed novel SMP foam exhibiting an open porous structure and the capacity to conform the irregular boundaries of bone defects.[19] The SMP foam was prepared on the basis of the photopolymerization of PCL diacrylate (PCLDA), coated with a mechanically stable polydopamine (PD) layer. After exposed to warm saline ($T_{saline} > T_m$ of PCLDA), the foam entered a temporary softened state and could be pressed into an irregular model defect to set shape.

Generally speaking, the ideal characteristic for the most biomedical applications is biodegradability to avoid second invasive surgery. Consequently, polycaprolactone, as an eco-friendly material,[20] which has good biodegradability, biocompatibility, chemical stability, thermal stability, and permeability,[21] is suitable

candidate for nerve cell tissue repair,[22] bone tissue repair,[23] and drug release carriers.[24] Meanwhile, the silk fibrin (SF) is naturally occurring fibrous proteins. Regarding the unique feature of reactive peptide, SF is a good direction for the development of biomedical devices with superior biocompatibility, high load capacity and a wide range of source.

So far, several foaming techniques have been employed to fabricate PCL foams, including gas blowing, selective laser sintering, solid state supercritical fluids foaming, particulate leaching, and phase separation. As for solid-state foaming method, it usually consists of mixing polymer powders and cross-linking agents, cold rolling and heating to generate both the formation of pores and polymerization. This method could eliminate foaming agent or liquid-treatment process, which is feasible to fabricate highly dense foams.

In this work, composite foams with shape-memory behavior were fabricated on the basis of biocompatible PCL and reinforced based on SF via solid state foaming method. SEM, DSC, DMA, and swelling equilibrium tests were applied to characterize basic properties of SMP foams with varying cross-linking agent content/reinforcement filler content, such as porosity and transitional temperature. Besides, compression tests at room temperature or high temperature were performed on shape-memory PCL foam and shape-memory composite foams. The effect of SF on shape-memory property and mechanical property was investigated.

EXPERIMENTAL

Foam Fabrication

Materials. PCL pellets were purchased from Perstorp Chemical Trading Co., Ltd. (CaPa 6500, M_n = 40 000~50 000; density: 1.146 g/mL). Benzoyl peroxide (BPO) was obtained from Changchun Jinghua Company, Changchun, China. Dichloromethane (CH_2Cl_2) was purchased from Tianjin Damao Chemical Reagent Factory, Tianjin, China. SF was procured from Shanghai Jianglaishiye Limited Company, Shanghai, China. All chemicals involved in preparing SMP composite foams were used as received.

SMP Foam Fabrication Method. In this study, solid-state foaming was selected as the foaming method to fabricate shape-memory PCL foams. The fabrication process (shown in Figure 1) can be described as following. First, a series of PCLs were dissolved into dichloromethane solvent with concentrations of BPO (BPO:PCL, 5; 10; 15; 20; and 25 wt%, respectively) was prepared. SFs were dissolved in PCL/BPO solution at concentration of 0.1, 0.2, and 15 wt%, respectively. The mixtures were dried at room temperature in an airing chamber for fabricating PCL films. Then, the PCL films will be cut into pieces with the size of 1.5 × 1.5 × 1 mm^3 for foaming. Finally, PCL pieces were placed into a suitable mold. After compacted and cured at 80°C for 3 h in oven, the composite PCL foams had been fabricated.

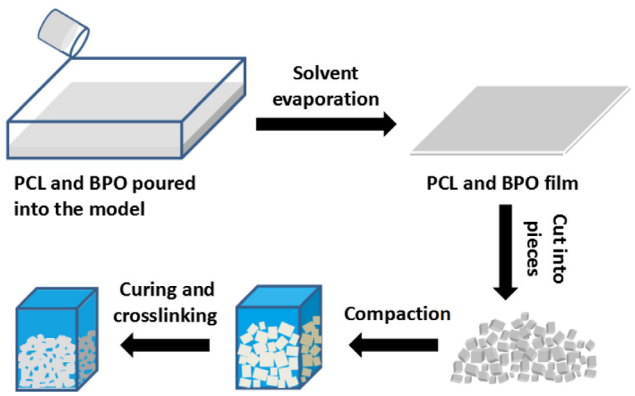

Figure 1. Illustration of fabrication of shape-memory foam. [Color figure can be viewed at wileyonlinelibrary.com]

Porosity and Pore Density of SMP Foam. Porosity: composite foam porosity (%) was calculated according to the following eq. (1)[25]:

$$Porosity\% = \left[1 - \left(\frac{\rho_F}{\rho_P}\right)\right] \times 100\% \quad (1)$$

Where ρ_p is the density of solid unfoamed polymer and ρ_F is the PCL foam determined via experimental measurement of weight at a certain dimension.

The pore density (N_f, volume occupied by the voids in per cm^3 of foam) was determined as[26]:

$$N_f = \frac{porosity}{(\pi/6) \times (pore\ diameter)^3} \quad (2)$$

Pore diameter was the average cell diameter in cm measured by ImageJ software from the SEM micrograph of foam.

Compression Test Measuring Modulus. The mechanical performance of the SMP composite foams were completed in Zwick/Roell testing system. The 0.1 N preload was set to ensure ideal contact between the clamp and composite foam specimen. The compressive tests were carried out at different temperatures: 20°C (room temperature), T_g-20°C, and 60°C [T_g], respectively.

Shape-Memory Behavior. Shape-memory properties of composite foams were quantified based on strain-controlled thermal mechanical compression test (Zwick/Roell). The effects of cross-linking agent, filler content, and foam-compression ratio on shape-memory effect were determined by the following sequence (shown in Figure 2): (1) compressed to a certain strain (ε_m = 40, 60, and 80%, respectively) after heating to T_g; (2) held at ε_m and cool to room temperature to fix the temporary shape; (3) measuring the height of specimen at 0, 0.166, 0.333, 0.5, 1, and 3 h, respectively, after removing the load; (4) reheated to T_g to recover the initial shape and measured the height of specimens after fully recovered.

The shape-fixity ratio (R_f) and shape-recovery ratio (η) were calculated by following equations:

$$R_f = \frac{\varepsilon}{\varepsilon_m} \times 100\% \quad (3)$$

$$\eta = \frac{h_t}{h_0} \times 100\% \quad (4)$$

Where ε is the fixed strain after cooling, ε_m is the maximum strain under load; h_0 and h_t is the height of initial specimen and recovered specimen, respectively.

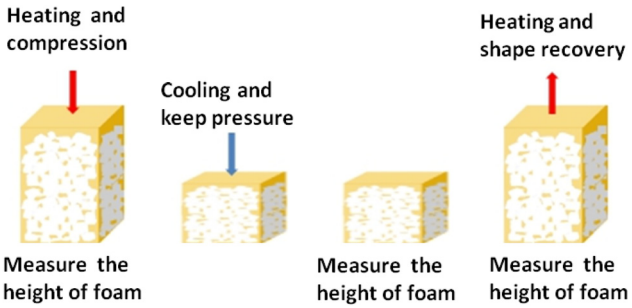

Figure 2. Schematic illustration of characterization procedure of shape-memory property of composite foams. [Color figure can be viewed at wileyonlinelibrary.com]

Differential Scanning Calorimetry. For thermal-responsive shape-memory materials, T_m or T_g plays a crucial role in influencing the shape-recovery behavior. In this study, Differential scanning calorimetry (DSC 204F1, Netzsch, Germany) was employed to investigate T_m of SMP composite foams in a nitrogen environment within a temperature range from 25 to 100°C at 10 °C min^{-1}.

The Pore Morphology of Composite Foam. Scanning electron microscopy (SEM, VEGA3 TESCAN) was employed to characterize the pore structure of the composite foam with varying cross-linking agent content. As a result of poor conductivity of sample, it was coated with Au prepared by sputter coating (KYKY-2800B, KYKY Technology Development Ltd.) for SEM analysis.

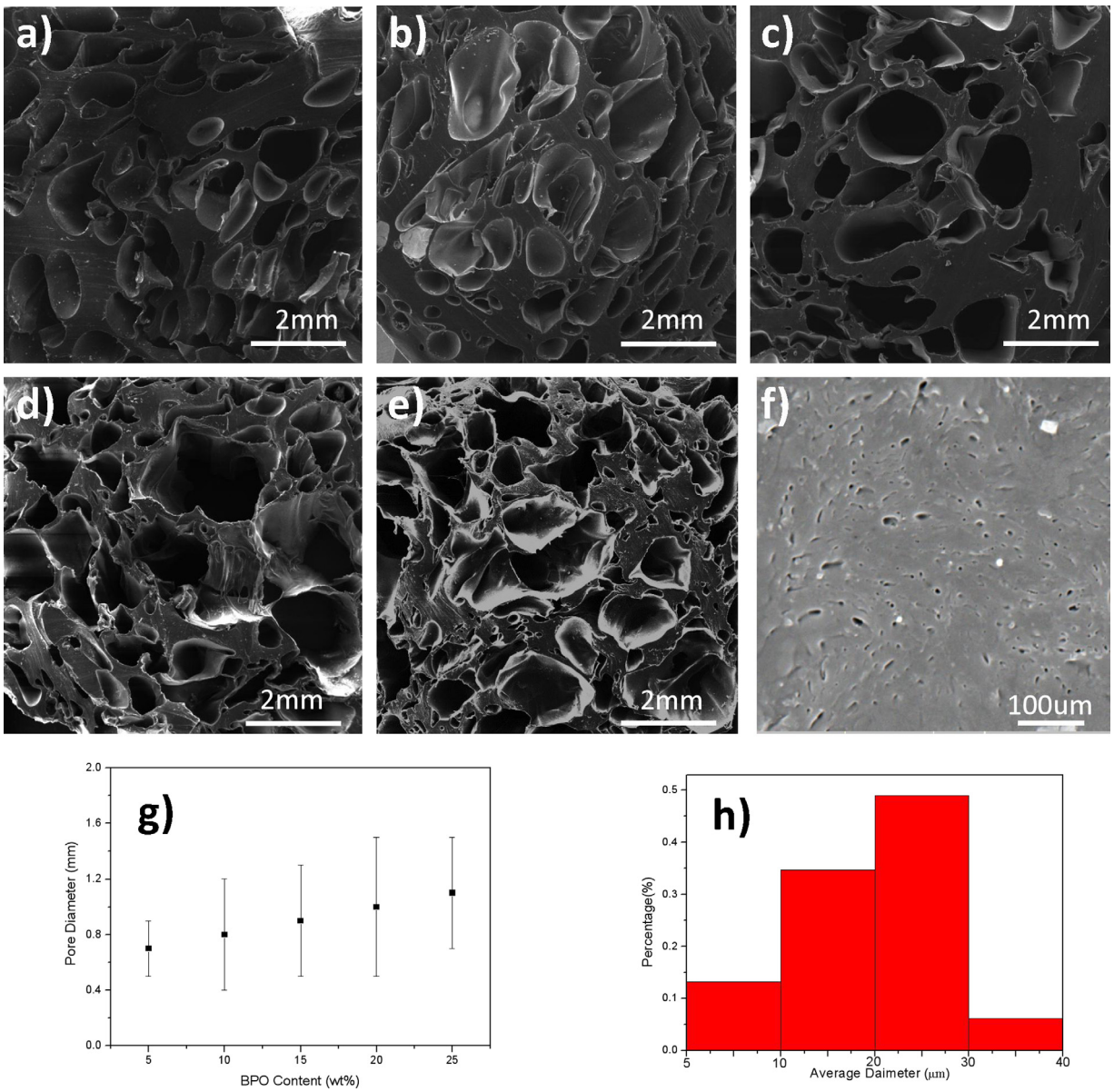

Figure 3. SEM images showing effect of concentration of cross-linking agent (BPO) on pore morphology (a) 5, (b) 10, (c) 15, (d) 20, and (e) 25 wt%, (f) micropore in the cell wall of shape+memory foam with 25 wt% BPO and (g, h) the average diameters of macropores and micropores, which were determined by ImageJ software. [Color figure can be viewed at wileyonlinelibrary.com]

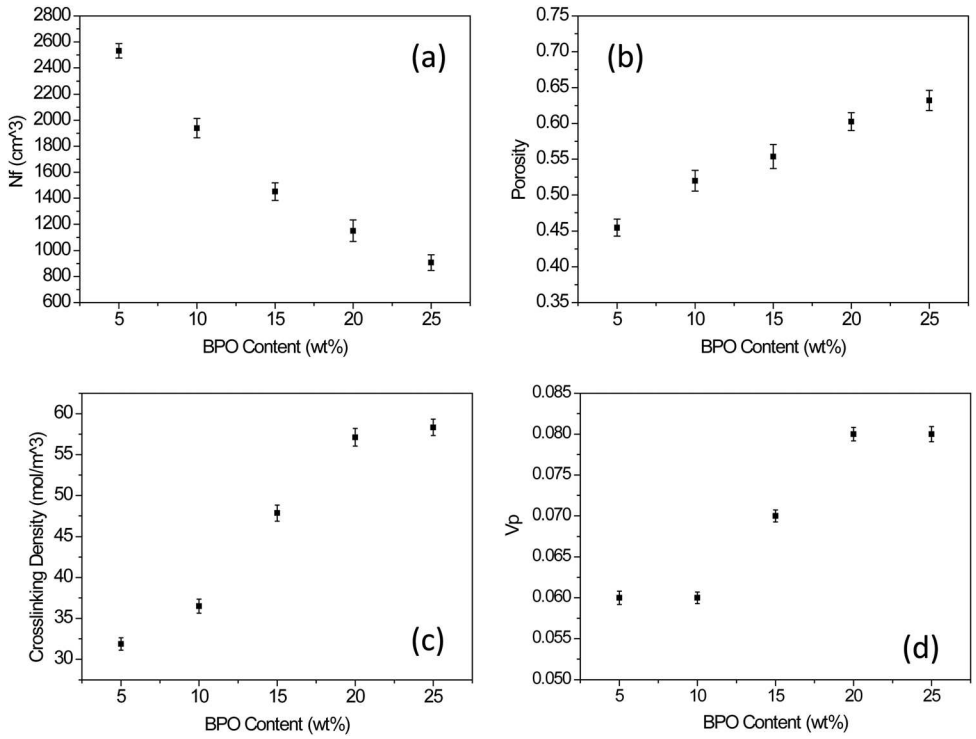

Figure 4. Performance parameters of SMP foams with varying BPO content: (a) pore density, (b) porosity, (c) cross-linking density, and (d) the equilibrium volumetric swelling ratio.

RESULTS AND DISCUSSION

Foam Microstructure

In order to investigate the effect of concentration of cross-linking agent (BPO) on the morphology of PCL foam, SEM was conducted in this study. Figure 3 showed the SEM images of PCL foam had different concentration of cross-linking agent BPO (5, 10, 15, 20, and 25 wt%, respectively). It showed that hierarchical cellular structures with uniform distribution in SMP foam were obtained. In this case, the big-size pore with regular shape depended on the PCL/BPO film cube with the same particle size. The size of pores was mainly determined by the reaction rate between PCL and BPO, related to the concentration of BPO. In Figure 3(a–c), the shape of pore was spherical or ellipsoidal and the size was relatively uniform. But in Figure 3(d,e), the pore structure was nonuniform and the wall of pore was relatively thin compared to that of foam with the lower BPO concentration. It was caused by the rapid and intense reaction during the foam formation at the high concentration of cross-linking agent condition. It showed the reasonable results that the average size increased from 0.7 to 1.1 mm with increasing the concentration of cross-linking agent (BPO) from 10 to 25 wt%, shown in Figure 3(g). Other kinds of micropore only appeared on the wall of big-pore cell, shown in Figure 3(f), which were caused by the released CO_2 from the reaction between PCL and BPO. The main dispersion range of the micropore diameter was around 10–30 μm, shown in Figure 3(h). Thus, such micropore appeared in all the foam with varying PBO content and the surface scratches and some particles were left behind when the material surface was polished.

Control Cellular Structure

From a design point of view, the foam mechanical property is determined by its structure and property of raw materials. The foam porosity and pore density are key parameters to determine the structure of foam. Figure 4(a,b) showed the pore density and porosity of foam were expressed as a function of concentration of BPO, respectively. The pore density decreased with the increasing of BPO concentration, although the increase of porosity was near linear as BPO concentration increasing. By comparing different composite foams, varying concentration of SF had no effect on the pore morphology, porosity, and pore density. Because there was no chemical reaction between SF and PCL matrix, no emission of gaseous products affected the foam morphology. Therefore, SF was not considered in this section. Figure 4(c,d) showed the cross-linking density and the volume ratio of polymer swelling equilibrium of PCL foams were expressed as a functional of BPO content, which was calculated according to Ref [18]. The cross-linking density and the volume ratio of polymer-swelling equilibrium slowly increased with the increase of cross-linker content from 5 to 10 wt% BPO, followed a rapid linearly increasing from 10 to 20 wt% BPO, and finally increased slowly to the maximum value at 25 wt%.

DSC Analysis

As for SMPs, T_g or T_m was a critical parameter in influencing its shape-recovery performance. Figure 5 indicated that the change in heat flow was expressed as a function of temperature for PCL foams, composite foams, and neat SF, respectively. The melting points of cross-linked PCL foams were 58.50, 57.67, 55.50, 52.50,

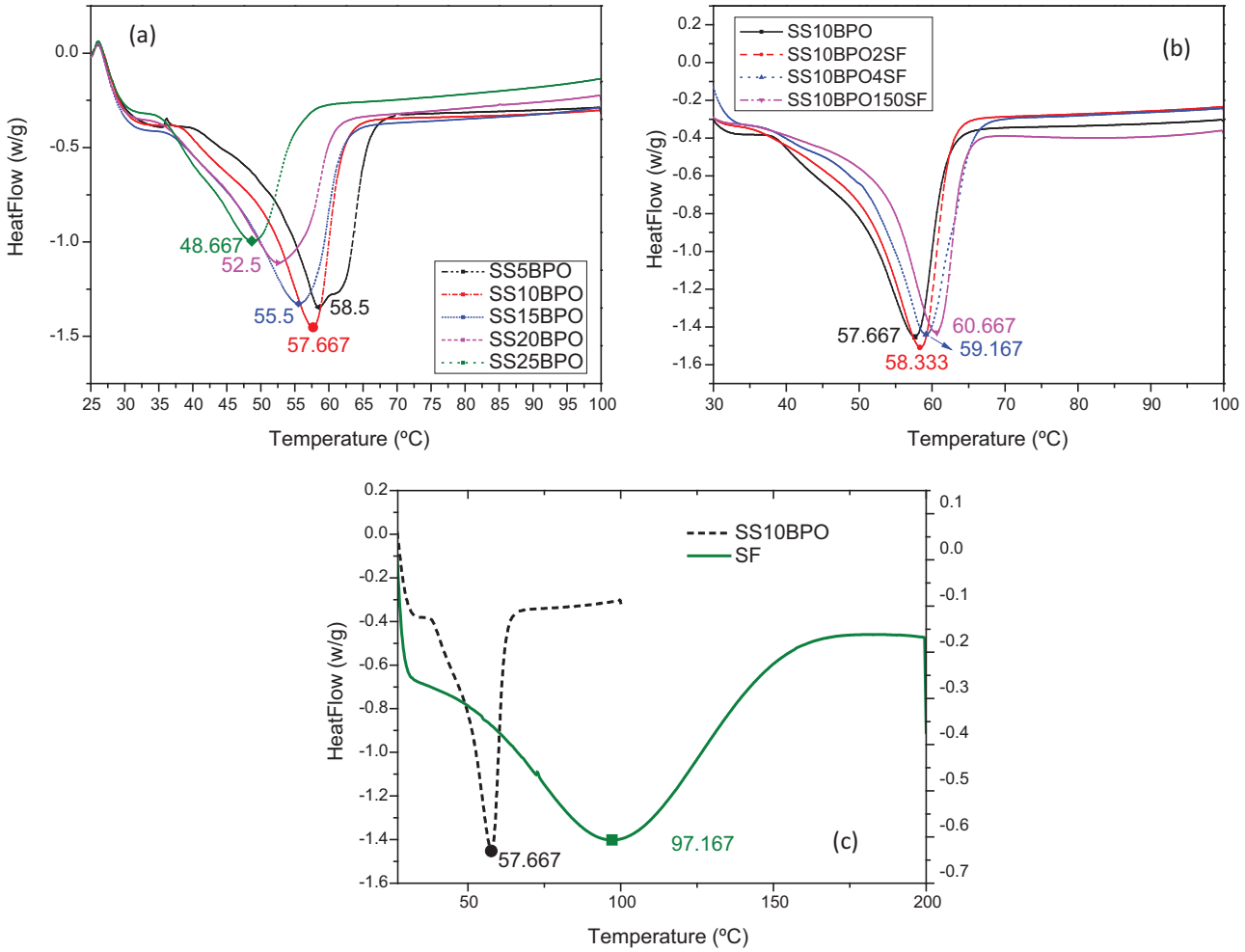

Figure 5. DSC of SMP foam specimens with (a) varying BPO content (5, 10, 15, 20, and 25 wt%, respectively) and (b) silk fibrion content (0.2, 0.4, 15 wt%, with 10 wt% BPO, respectively), and (c) pure silk fibrion and PCL foam with 10 wt% BPO. [Color figure can be viewed at wileyonlinelibrary.com]

and 48.67°C for 5, 10, 15, 20, and 25 wt% BPO, respectively. It decreased as the concentration of cross-linking agent BPO increased. It may be interpreted that rising BPO content leading to the increase cross-linking density will impede the creation of crystal, which resulted in the decease melting temperature.

As for SF enhanced composite foams, however, PCL with 10 wt% BPO, T_m was shifted to a higher temperature as SF content increase, which were 57.67, 58.33, 59.17, and 60.67°C for 0, 0.2, 0.4, and 15wt% SF, respectively. T_m of neat SF was 97.17°C, shown in Figure 5(c). Such enhanced T_m of composite foam may be related to much higher T_m of SF compared with PCL matrix.

Compressive Modulus at Different Temperatures

The effect of cross-linker content and SF filler on the mechanical properties of the foams was studied through uniaxial compression tests, which was shown in Figure 6. Compared with conventional foams, shape-memory foams showed similar regions of the force-distance compression curves: linear-elastic region, pores collapse/cell wall bending, and densification (cell walls are compressed together). Figure 6(a) showed that the increase in the concentration of BPO produced the significant change in effective elastic modulus of foam. As shown in Figure 4(c), the increased cross-linker concentration was leading to the increasing of cross-linking density, which made cell-walls stronger; but, it also arose porosity and pore density of foam, which was the main factor for decreasing foam elastic modulus [shown in Figure 4(b)]. Figure 6(b) presented that effective elastic modulus of foams were significantly enhanced as the increasing of SF filler content from 0.2 to 7.5%, although it decreased when SF concentration was greater than 7.5%. To conclude, in a certain concentration range, the effective elastic modulus could be improved by the increase of SF; yet excessive SF hindered the cross-linking degree of BPO and PCL, which weakened the foam mechanical properties (shown in Figure 6(b)).

Because SMP foams are variable stiffness materials, the mechanical properties at different temperatures are very important for determining their practical engineer applications. Figure 6(c,d) showed effective elastic modulus of foams versus temperatures (room temperature, T_g-20°C and 60°C[T_g], respectively). For effective elastic modulus of foams at higher temperature (> room temperature), the similar trends had been observed for both increasing of BPO concentration and SF filler, except the temperatures higher than T_g. Because composite foams would change from elastic state to viscoelastic state when the temperature reached to T_g / >T_g.

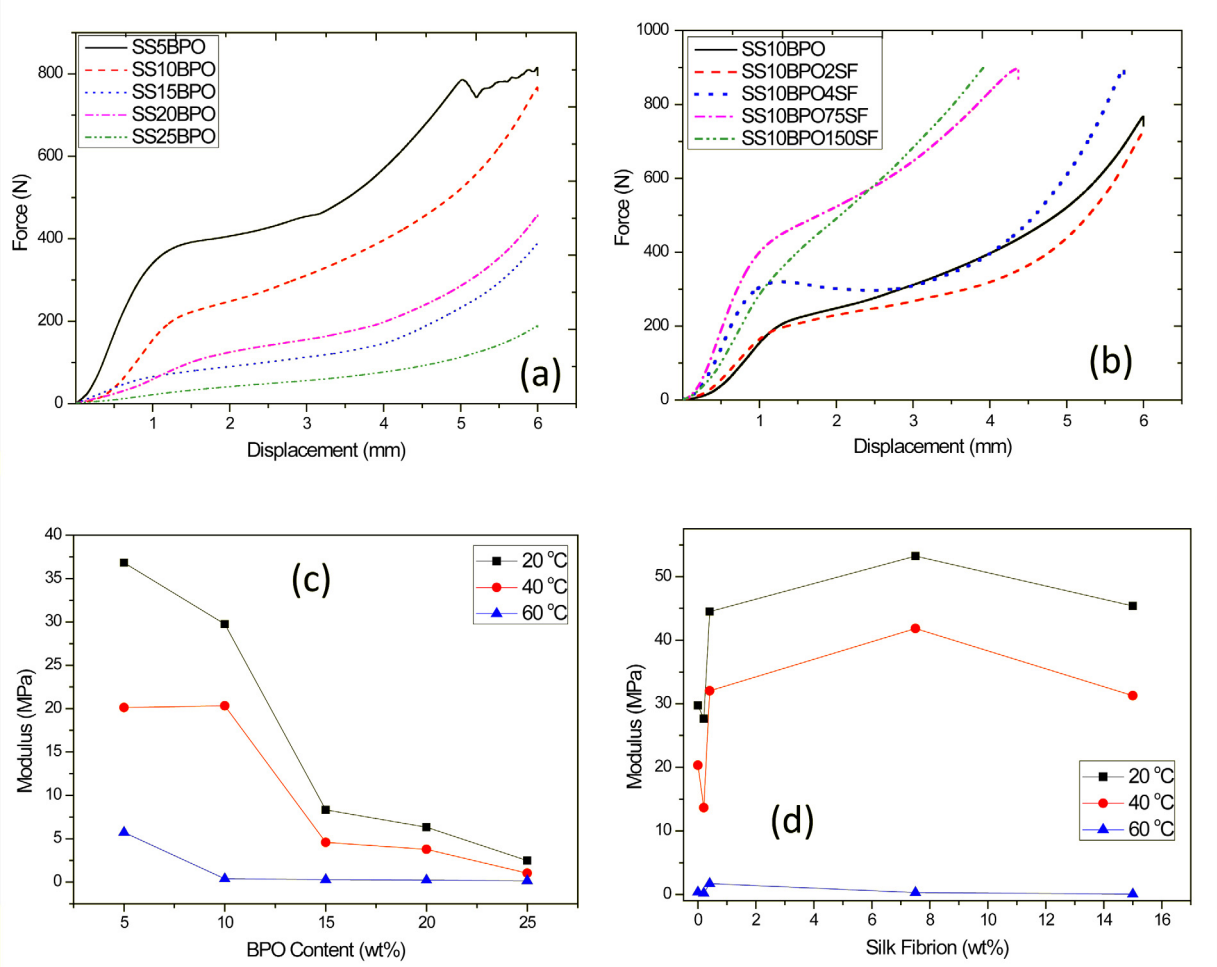

Figure 6. Compression tests under different temperatures: (a) foam with varying BPO content (5, 10, 15, 20, 25 wt%, respectively) at room temperature; (b) foam (10 wt% BPO) with varying SF content (0.2, 0.4, and 15 wt%, respectively) at room temperature; (c,d) modulus of PCL foam with varying BPO content (5, 10, 15, 20, and 25 wt%, respectively) and composite foam with varying SF content (0.2, 0.4, 15, with 10 wt% BPO, respectively) under different temperature (20, Tg-20, and 60°C(Tg), respectively). [Color figure can be viewed at wileyonlinelibrary.com]

Shape Memory Property

Figure 7 showed the shape-fixing ratios of PCL foams and composite foams (under the compression of 40 60, and 80%, respectively) were functional of time. The more compressed the foams, the larger the deformation of cell walls, and the higher the internal stress. Thereby, if shape-memory foams could not fix the residual stress, it would release the stress by expanding, in order to balance out the system when the temperature dropped. In this case, ensure to get more accurate shape-fixity ratio, the length of fixed foams had been measured at 0, 0.166, 0.333, 0.5, 1, and 3 h, after removing the load. As Figure 7 shown, the shape-fixing ratio decreased with time in the first-half hour and stayed the same after 3 h. As for PCL foams and composite foams, the shape-fixing ability was improved with the increase of the compression ratio, and the maximum value (100%) was observed under the compression of 80%, except the foam with 25 wt% BPO. For compression of 40 and 60%, the lowest shape-fixity ratio (around 87.4%) was observed at the highest cross-linking agent content (25 wt% BPO) of PCL foam, whereas a relatively higher shape-fixity ratio (R_f > 98.5%) was obtained at the lower BPO content (<20 wt%). A higher BPO content increased the cross-linking density, leading to the stronger modulus of cell wall and the lower shape-fixity ratio. However, there was no obvious difference for the fixing ratio trends of composite foams with varying addition of SF (in the range of 0.2 wt%), comparing with that of PCL foams.

Figure 8 indicated that shape-recovery ratio was expressed as the function of addition content of SF in composite foams. The good shape-recovery ratio (η > 97.6%) was obtained without SF addition and decreased with the increase of SF addition in composite foams. The SF had relative higher melting temperature (97°C) compared with PCL matrix (around 60°C), which induced that the response of SF component could not synchronize with that of PCL matrix at the stimuli temperature of 60°C. On the other hand, addition of SF in PCL matrix had a negative effect on the degree of PCL crosslinking and impeded the movement of PCL chain during the shape-recovering process. Thereby, the shape-recovery ratio also decreased as increasing-compression ratio of composite foams according to thermoplastic deforming of SF during shape-fixing process at 60°C.

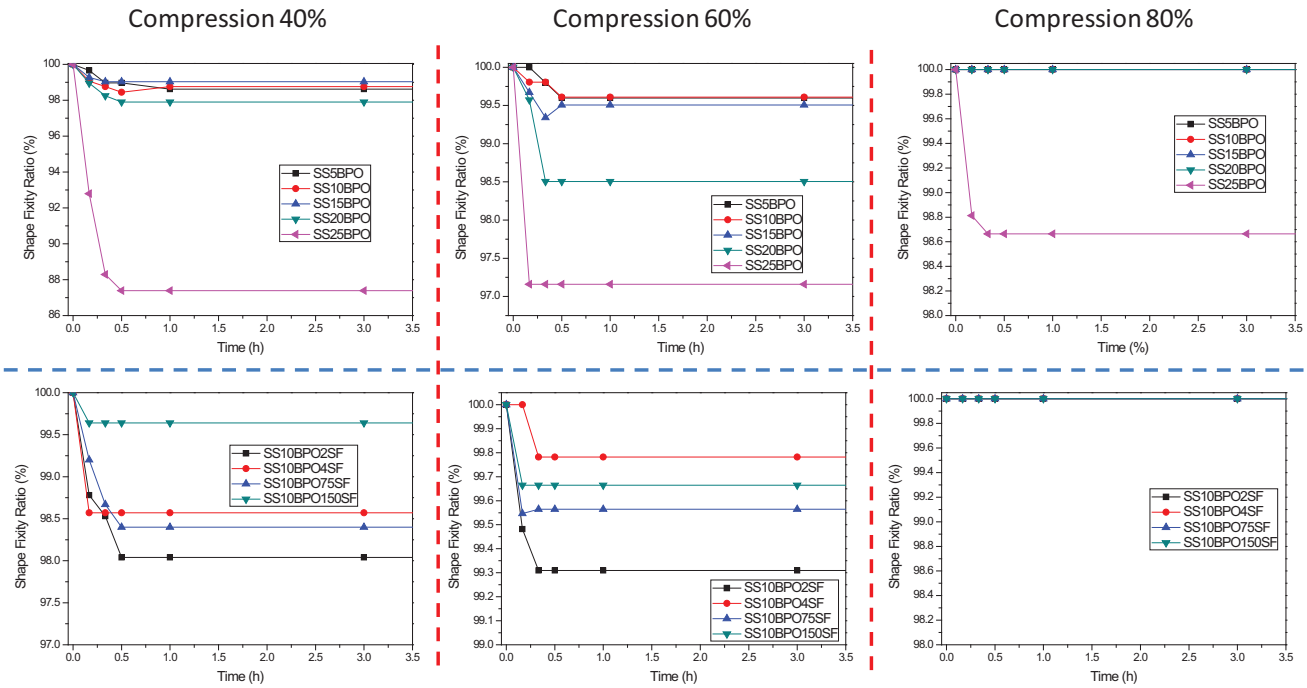

Figure 7. Shape-fixity ratio of PCL foam and composite foam under compression of 40, 60, and 80%, respectively. [Color figure can be viewed at wileyonlinelibrary.com]

CONCLUSION

In summary, a type of composite foam with shape-memory property had been developed on the basis of biocompatible PCL and SF through solid state foaming method. As for the composite foam, the porosity and pore density were mainly related to the content of cross-linking agent (BPO). The pore density decreased with the increasing of concentration of BPO, although porosity was near linear increasing as BPO content increasing. SF had no effect on the pore morphology. As for the stimulus temperature of composite foam, it reduced with BPO increasing and improved with addition of SF. Effective elastic modulus decreased as the concentration of crosslinking agent increasing and improved greatly by adding the content of SF increasingly. For both PCL foam and SF reinforced composite foam, shape-recovery tests were performed as well. The results of shape-fixity ratio and recovery ratio showed that the shape memory of PCL foams had great shape-memory properties compared with the composite foam.

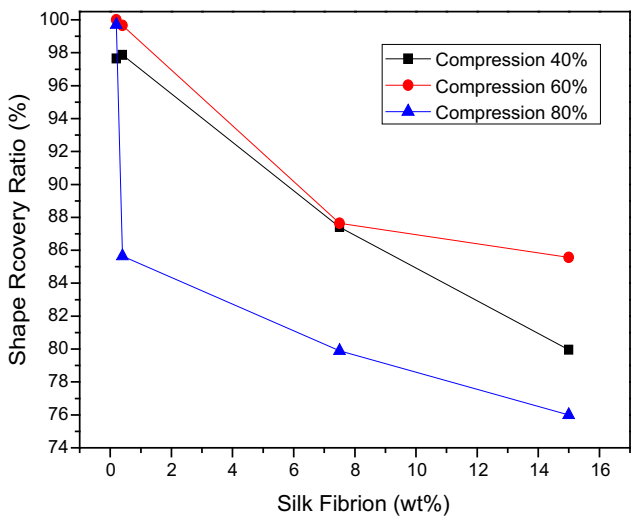

Figure 8. Shape-recovery ratio of composite foam under compression of 40, 60, and 80%, respectively. [Color figure can be viewed at wileyonlinelibrary.com]

ACKNOWLEDGMENTS

This research was supported by the National Natural Science Foundation of China [grant No. 11772108 and 11632005].

REFERENCES

1. Lu, H.; Yao, Y.; Lin, L. *Pigm. Resin Technol.* **2015**, *44*, 94.
2. Wang, Y.; Tian, W.; Zhu, G. *J. Nanosci. Nanotechnol.* **2017**, *1*, 3373.
3. Lu., H.; Yao, Y.; Lin, L. *Pigm. Resin Technol.* **2014**, *43*, 26.
4. Lu, H.; Yao, Y.; Yin, J.; Lin, L. *Pigm. Resin Technol.* **2016**, *45*, 93.
5. Lu, H.; Yao, Y.; Zhang, A.; Lin, L. *Pigm. Resin Technol.* **2015**, *45*, 62.
6. Luo, H.; Li, Z.; Yi, G.; Zu, X.; Wang, H.; Huang, H.; Wang, Y.; Liang, Z.; Zhang, S. *Mater. Lett.* **2014**, *137*, 385.
7. Luo, H.; Zhoua, X.; Ma, Y.; Yi, G.; Cheng, X.; Zhu, Y.; Zu, X.; Zhang, N.; Huang, B.; Yu, L. *Appl. Surf. Sci.* **2016**, *363*, 59.

8. Dong, Y.; Xia, H.; Zhu, Y. F.; Ni, Q.; Fu, Y. *Compos. Sci. and Technol.* **2015**, *120*, 17.
9. Dong, Y.; Ni, Q.; Fu, Y. *Compos. Part A*. **2015**, *72*, 1.
10. Lu, H.; Yao, Y.; Lin, L. *Pigm. Resin Technol.* **2015**, *44*, 244.
11. Santo, L. *Prog. Aerosp. Sci.* **2016**, *81*, 60.
12. Santo, L.; Quadrini, F.; Villadei, W.; Mascetti, G.; Zolesi, V. *Procedia Engineering*. **2015**, *104*, 50.
13. Zhang, D.; Petersen, K. M.; Grunlan, M. A. *ACS Appl. Mater. Inter.* **2013**, *5*, 186.
14. Zhang, F.; Zhou, T.; Liu, Y.; Leng, J. *Sci. Rep.* **2015**, *5*, 11152.
15. Rodriguez, J. N.; Clubb, F. J.; Wilson, T. S.; Miller, M. W.; Fossum, T. W.; Hartman, J.; Tuzun, E.; Singhal, P.; Maitland, D. J. *J. Biomed. Mater. Res.* **2014**, *102*, 1231.
16. Ortega, J.; Hartman, J.; Rodriguez, J.; Maitland, D. J. *An Biomed. Eng.* **2013**, *41*, 725.
17. Song, J. J.; Chang, H. H.; Naguib, H. E. *Polymer*. **2015**, *56*, 82.
18. Muschenborn, A. D.; Ortega, J. M.; Szafron, J. M.; Szafron, D. J.; Maitland, D. J. *BioM. Eng. OnLine*. **2013**, *12*, 103.
19. Zhang, D.; George, O. J.; Petersen, K. M.; Jimenez-Vergara, A. C.; Hahn, M. S.; Grunlan, M. A. *Acta Biomater.* **2014**, *10*, 4597.
20. Peponi, L.; Navarro-Baena, I.; Sonseca, A.; Gimenez, E.; Marcos-Fernandez, A.; Kenny, J. M. *Euro. Polym. J.* **2013**, *49*, 893.
21. Woodruff, M. A.; Hutmacher, D. W. *Prog. Polym. Sci.* **2010**, *35*, 1217.
22. Song, X.; Wei, Y.; Li, G.; Qin, W.; Wang, W.; Zhang, X.; Zhao, H. *Chinese J Rep Reconstr Surg*. **2016**, *5*, 646.
23. Zhang, X.; Song, X.; Wang, W.; Li, Z.; Zhao, H. *Chinese J Rep Reconstr Surg*. **2016**, *5*, 638.
24. Dash, T. K.; Konkimala, B. *Mol. Pharm.* **2012**, *9*, 2365.
25. Salerno, A.; Iannace, S.; Netti, P. A. *Macromol. Biosci.* **2008**, *8*, 655.
26. Kumar, V.; Suh, N. P. *Polym.. Eng.. Sci.* **1990**, *30*, 1323.